Changes in the FXR-cistrome and alterations in bile acid physiology in Wilson disease

VISUAL ABSTRACT

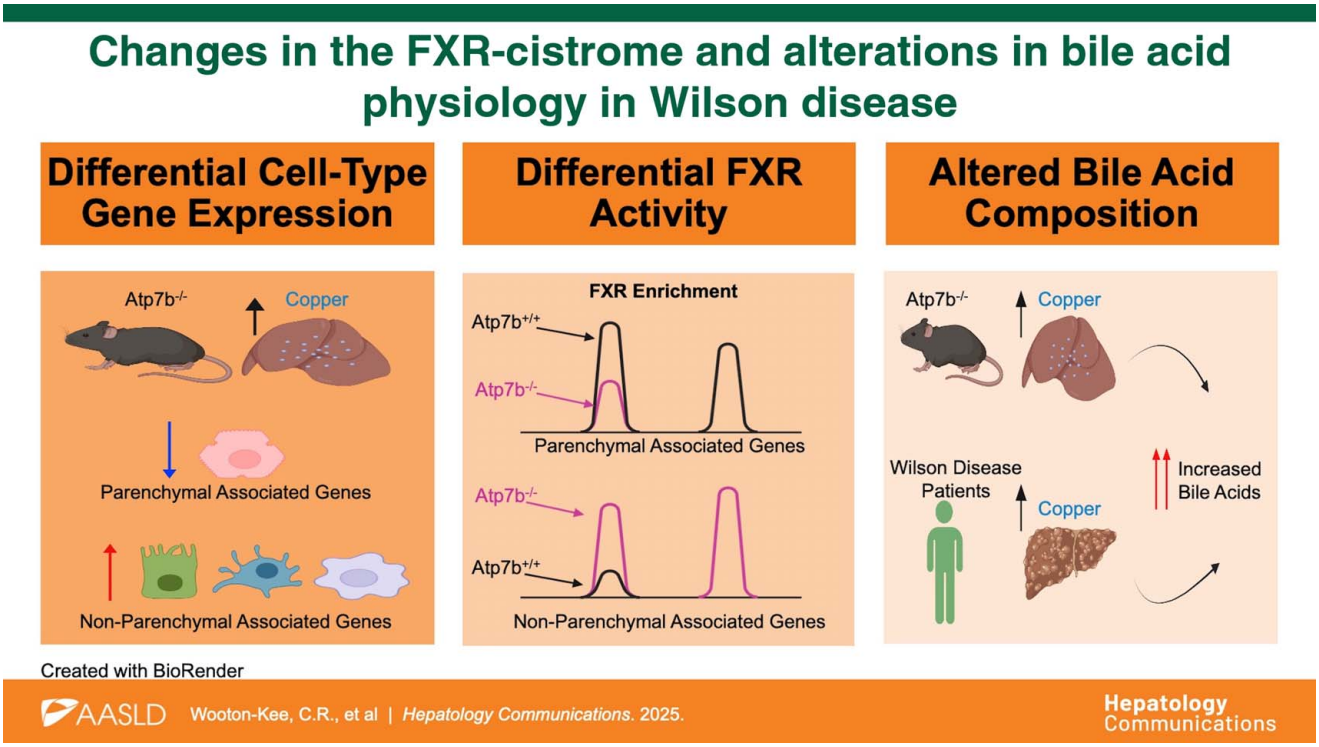

Received: 12 November 2024 | Accepted: 22 February 2025

DOI: 10.1097/HC9.0000000000000707

ORIGINAL ARTICLE

OPEN

Changes in the FXR-cistrome and alterations in bile acid physiology in Wilson disease

Clavia Ruth Wooton-Kee[1,2] | **Hari K. Yalamanchili**[1,3] | **Islam Mohamed**[4] | **Manal Hassan**[5] | **Kenneth D.R. Setchell**[6,7] | **Monica Narvaez Rivas**[6,7] | **Ayse K. Coskun**[8] | **Vasanta Putluri**[2,9] | **Nagireddy Putluri**[2] | **Prasun Jalal**[4] | **Michael L. Schilsky**[8] | **David D. Moore**[10]

[1]Department of Pediatrics-Nutrition, Children's Nutrition Research Center, Baylor College of Medicine, Houston, Texas, USA

[2]Department of Cellular and Molecular Biology, Baylor College of Medicine, Houston, Texas, USA

[3]Department of Pediatrics-Neurology, Jan and Dan Duncan Neurological Research Institute, Texas Children's Hospital, Houston, Texas, USA

[4]Department of Internal Medicine, Baylor College of Medicine, Houston, Texas, USA

[5]Department of Epidemiology, Division of Cancer Prevention and Population Sciences, MD Anderson Cancer Center, Houston, Texas, USA

[6]Division of Pathology and Laboratory Medicine, Cincinnati Children's Hospital, Cincinnati, Ohio, USA

[7]Department of Pediatrics, University of Cincinnati College of Medicine, Cincinnati, Ohio, USA

[8]Department of Medicine and Surgery, Yale School of Medicine, New Haven, Connecticut, USA

[9]Advanced Technology Core, Dan Duncan Cancer Center, Baylor College of Medicine, Houston, Texas, USA

[10]Department of Nutrition Sciences and Toxicology, University of California, Berkeley, Berkeley, California, USA

Correspondence
Clavia Ruth Wooton-Kee, Department of Pediatrics-Nutrition, Children's Nutrition Research Center, Baylor College of Medicine, 1100 Bates Avenue, Houston, TX 77030, USA.
Email: wootenke@bcm.edu

Abstract

Background: Wilson disease (WD) is an autosomal recessive disorder that results in excessive hepatic copper, causing hepatic steatosis, inflammation, fibrosis, cirrhosis, and liver failure. Previous studies have revealed dysregulation of many farnesoid X receptor (FXR) metabolic target genes in WD, including the bile salt exporter pump, the major determinant of bile flow.

Methods: We tested the hypothesis that the FXR-cistrome is decreased in *Atp7b*$^{-/-}$ mice in accord with dysregulated bile acid homeostasis.

Results: FXR binding within *Atp7b*$^{-/-}$ mouse livers displayed surprising complexity: FXR binding was increased in distal intergenic regions but

Abbreviations: Atp7b, ATPase copper transporting beta; BCM, Baylor College of Medicine; Bsep, bile salt exporter pump; CDCA, chenodeoxycholic acid; DEG, differentially expressed gene; ERα, estrogen receptor alpha; FC, fold change; FDR, false discovery rate; FGF15, fibroblast growth factor 15; FXR, farnesoid X receptor; GCA, glycocholic acid; G-CDCA, glycochenodeoxycholic acid; GO, Gene Ontology; G-UDCA, glycourosodeoxycholic acid; IGV, Integrative Genomics Viewer; KEGG, Kyoto Encyclopedia of Genes and Genomes; LEC, Long-Evans Cinnamon; MASLD, metabolic dysfunction–associated steatotic liver disease; MDACC, MD Anderson Cancer Center; MVECS, multivesicular endothelial cells; PPAR, peroxisome proliferating receptor; SHP, short heterodimer partner; T-CA, taurocholic acid; T-CDCA, taurochenodeoxycholic acid; T-MCA, tauromuricholic acid; T-UDCA, tauroursodeoxycholic acid.

Supplemental Digital Content is available for this article. Direct URL citations are provided in the HTML and PDF versions of this article on the journal's website, www.hepcommjournal.com.

decreased in promoter regions in *Atp7b*$^{-/-}$ versus wild-type mice. Decreased FXR occupancy in *Atp7b*$^{-/-}$ versus wild-type mice was observed in hepatocyte metabolic and bile acid homeostasis pathways, while enrichment of FXR binding was observed in pathways associated with cellular damage outside of hepatocytes. Indeed, disparate FXR occupancy was identified in parenchymal and non-parenchymal marker genes in a manner that suggests decreased FXR activity in parenchymal cells, as expected, and increased FXR activity in non-parenchymal cells. Consistent with altered FXR function, serum and liver bile acid concentrations were higher in *Atp7b*$^{-/-}$ mice than in wild-type mice. Comparison of bile acid profiles in the serum of WD patients with "liver," "neurological," or "mixed" disease versus healthy controls also revealed increases in specific bile acids in WD-liver versus healthy controls. **Conclusions:** We identified novel FXR-occupancy across the genome that varied in parenchymal and non-parenchymal cells, demonstrating complex FXR regulation of metabolic and hepatocellular stress pathways in *Atp7b*$^{-/-}$ mice. Dynamic changes in FXR activity support our novel finding of altered bile acid metabolism in *Atp7b*$^{-/-}$ mice and WD patients.

Keywords: bile acids, copper, FXR, nuclear receptors, Wilson disease

INTRODUCTION

Copper is an essential trace mineral acquired from the diet. Copper homeostasis is maintained primarily in the liver and requires the transmembrane copper-transporting P-type ATPase ATP7b for either systemic secretion (in complex with ceruloplasmin) or elimination from the body via removal in bile. Mutations in ATP7B result in Wilson disease (WD), an autosomal recessive disorder with an occurrence of ~1:30,000.[1] Although WD patients may present with a variety of neurological symptoms, such as tremors, dystonia, and psychiatric disorders, most develop primarily hepatic symptoms, such as steatosis, jaundice, hepatitis, and liver failure.[2] The heterogeneity of symptoms complicates WD diagnosis, highlighting the need for more mechanistic studies.

Excess copper has a negative impact on nuclear receptors, a group of transcription factors that contain a ligand binding domain that confers specificity for activation and a highly conserved zinc-finger DNA binding domain that is required for binding to nuclear receptor response elements of target genes.[3] In vitro studies with estrogen receptor demonstrated that copper could displace zinc in the DNA binding domain, resulting in a highly disordered DNA binding domain structure and loss of estrogen receptor binding to estrogen response elements.[4,5] Similarly, in vitro and in vivo studies demonstrated similar effects of excess copper on hepatic metabolic nuclear receptors (FXR, LRH1, and HNF4α) in WD.[6] These studies suggest a link between impaired nuclear receptor function and changes in metabolite composition in WD.

Changes in nuclear receptor activity are correlated with metabolic alterations in patients with WD and in animal models. Both WD patients and *Atp7b*$^{-/-}$ mice have altered lipid metabolism as well as differential enrichment of amino acids, tricarboxylic acid cycle, glycolytic, and bile acid intermediates.[7–15] Metabolic changes coincide with transcriptomic alterations in *Atp7b*$^{-/-}$ mice[12] and Long-Evans Cinnamon (LEC) rats,[15] which include decreased mRNA expression of genes involved in hepatic metabolic homeostasis.[3,6,10–12] It is plausible that some of these altered metabolites, such as bile acids and free fatty acids, are endogenous ligands for the residual pool of nuclear receptors (such as FXR and PPARα) that are not inactivated in cells with excess copper. The precise mechanisms regulating these metabolic changes and the downstream consequences of the altered metabolome are not fully understood and are likely the result of both the direct and indirect effects of copper.

Bile acids are amphipathic molecules that not only promote the emulsification and absorption of lipid-soluble nutrients but also have endocrine signaling properties. In the liver, bile acids are critical regulators of their own formation and secretion. Enterohepatic regulation of FXR signaling is mediated via induction of the fibroblast growth factor 15 (mice)/fibroblast growth factor 19 (humans) mRNA expression in the ileum.[16] Fgf15/Fgf19 subsequently binds to FGFR4/β-Klotho receptors in hepatocytes, leading to

repression of Cyp7a1 expression and reduced bile acid synthesis.[16] This regulatory feedback loop mitigates bile acid toxicity by reducing bile acid synthesis. Endogenous bile acids [chenodeoxycholic acid (CDCA)] are potent ligands for the nuclear receptor farnesoid X receptor (FXR, NR1H4), and FXR activation increases expression of short heterodimer partner (SHP, NR0B2),[17,18] which promotes the formation of co-repressor complexes with LRH1 on the promoters of *Cyp7a1*, *Cyp8b1*, and *Ntcp*, resulting in decreased bile acid synthesis and uptake.[19–21] Dysregulation of bile acid metabolism in WD patients and animal models is in agreement with previous reports describing the negative impact of copper on FXR and other nuclear receptor signaling.[3]

In the current study, we provide detailed transcriptomic, FXR-cistromic, and bile acid composition of *Atp7b*$^{-/-}$ mice as well as the bile acid composition of WD patients. Our findings demonstrate global alterations in FXR signaling that overlap with metabolic transcriptomic signatures and bile acid metabolism. Our cistromic analyses suggest that FXR function is impaired in hepatocytes, as expected, but may be increased in non-parenchymal cells. We found that WD patients with liver, neurological, and mixed (neurological and liver) symptoms have differential bile acid composition profiles. Taken together, this comprehensive analysis of changes in bile acid signaling and physiology shows that both *Atp7b*$^{-/-}$ mice and WD patients with liver disease have alterations in bile acid homeostasis.

METHODS

Animal care

Male Atp7b$^{-/-}$,[10] *FXR*$^{-/-}$,[22] DKO$^{Atp7b:FXR}$, and wild-type (WT) mice on C57BL/6 background were fed a standard laboratory chow diet ad libitum, maintained on a 12-h light–dark cycle, and euthanized at Zeitgeber time 2–3. All mice were bred and maintained in the Baylor College of Medicine (BCM) animal facility. *Atp7b*$^{-/-}$ and WT mice were generated from *Atp7b*$^{+/-}$ mating pairs. Atp7b$^{-/-}$ and *FXR*$^{-/-}$ mice were crossed to generate the DKO$^{Atp7b:FXR}$ mice. Both *FXR*$^{-/-}$ and DKO$^{Atp7b:FXR}$ were generated from either homozygous *FXR*$^{-/-}$ or double homozygous DKO$^{Atp7b:FXR}$ mating pairs. All animal experiments were performed according to the guidelines detailed in the Guide for the Care and Use of Laboratory Animals[23] and were approved by the Institutional Animal Care and Use Committee at BCM.

Real-time PCR and RNA-sequencing analysis

RNA was harvested from 6-month-old male WT and *Atp7b*$^{-/-}$ mice using TRIzol Reagent (Invitrogen) and RNeasy kit (Qiagen). Primers used for real-time PCR have been previously described.[6,10] RNA-sequencing with the NextSeq Illumina 500/550 Mid Output v2 kit (300 cycles) was performed at the Genomics Core at the Children's Nutrition Research Center at BCM.

Sequencing quality and adapter contamination were assessed using FastQC. Any adapter sequences were trimmed using Cutadapt. Reads were aligned to the *Mus musculus* genome (mm10) reference genome using STAR. Gene expression values from each sample were quantified as the number of reads mapped (to a specific gene) by setting–quantMode to GeneCounts in STAR. Genes with an average read count <50 across the samples were considered not expressed and excluded from the differentially expressed gene (DEG) analysis. Raw read counts were normalized and then tested for differential expression using DESeq2.[24] A false discovery rate (FDR) cutoff of 0.05 and a fold change cutoff of 20% ($-0.263 \leq \log_2(FC) \geq +0.263$) were used to call DEGs.

FXR ChIP sequencing analysis

ChIP sequencing was performed with 100 mg of liver tissue from 6-month-old *Atp7b*$^{-/-}$ and WT mice ($n=3$ mice/group) using the FXR antibody (H-130X, Santa Cruz Biotechnologies). ChIP-seq and initial data processing were carried out using the Active Motif analysis pipeline. The generated 75-nt single-end (SE75) reads were mapped to the *Mus musculus* genome (mm10) using the BWA algorithm with default parameters, and alignment data for each read was stored in BAM format. PCR duplicates were removed to ensure data quality. ChIP samples were normalized to their respective input controls and converted to bigWig format for visualization in the Integrative Genomics Viewer (IGV). Since the 5′-ends of the aligned reads mark the end of ChIP/IP fragments, tags were extended in silico to 200 bp at their 3′-ends to match the average fragment length of the size-selected library (performed with Active Motif software). For genome-wide fragment density calculation, the genome was divided into 32-nt bins, and fragment counts per bin were stored in bigWig files. Peak calling was conducted on individual replicates using MACS2,[25] with peaks from multiple samples grouped into "Merged Regions," defined by the most upstream and downstream coordinates among overlapping peaks. If only one sample contained a peak, that interval defined the Merged Region. DESeq2[24] was applied to normalize read counts across merged peak regions and perform differential peak analysis. Peaks were annotated and visualized using ChIPseeker.[26] Peaks were assigned to genes if they were located within 10 kb upstream of the transcription start site or downstream to the transcription end site. Promoter peaks were defined as those located within 10 kb upstream of the transcription start site. Mouse

liver-specific enhancer regions were downloaded from EnhancerAtlas 2.0.[27] Peaks overlapping by at least 1 nucleotide with these enhancers were annotated as enhancer peaks.

Bile acid measurements

Liver and serum bile acid measurements were performed at the BCM Metabolomics Core, as previously described, using the Biocrates Bile Acids kit[28] and UPLC-MS/MS.[29] Serum bile acid measurements in human samples were performed at the Clinical Mass Spectrometry Facility, Division of Pathology and Laboratory Medicine, Cincinnati Children's Hospital.

Human samples

Patient demographics and diagnoses are described in Supplemental Table S4, http://links.lww.com/HC9/B997. Patients (either new or follow-up) with metabolic dysfunction–associated steatotic liver disease (MASLD) visited BCM St. Luke's Liver Clinic and were diagnosed with MASLD either through imaging or liver biopsy. The control group consisted of relatives of cancer patients who visited the MD Anderson Cancer Center (MDACC). Since they share similar dietary habits and lifestyles with patients with cancer, they were screened for metabolic syndrome characteristics. WD patient samples were obtained from the Wilson disease registry study (Yale, data coordinating center). Studies conducted with human samples were approved by the Baylor College of Medicine IRB (H-30733 and H-45208) and were conducted following the Declaration of Helsinki and Istanbul. Data was obtained with de-identified human specimens, and the research was granted a waiver of informed consent.

Statistical analysis

Statistical analysis was performed using the GraphPad Prism software (v7.0). Data are presented as the mean ± SEM, and statistical significance was set at $p < 0.05$. Students *t* test was used to compare the differences between the 2 groups. For multiple group comparisons, one-way ANOVA tests followed by the Dunnett post hoc test were performed.

RESULTS

Changes in the transcriptome of *Atp7b*$^{-/-}$ mice

Studies in our laboratory, as well as others, have found dramatic alterations in the transcriptomic profiles of 6-week and 3-month-old presymptomatic *Atp7b*$^{-/-}$ mice.[10,12] We expanded these studies to include 6-month-old *Atp7b*$^{-/-}$ mice with moderate hepatocellular pathology (previously described[10]) to assess changes in gene signatures associated with increasing age and hepatic pathology. Hepatic transcriptomic profiles and DEGs in *Atp7b*$^{-/-}$ and age-matched WT mice were obtained by RNA-sequencing analysis (Figure 1A, Supplemental Table S1A, http://links.lww.com/HC9/B995). The most significantly upregulated DEGs were largely associated with changes in cell cycle regulation, cell growth and proliferation, and the response to metals (Figure 1A). Conversely, genes involved in metabolism were the most significantly downregulated DEGs, including the tricarboxylic acid cycle gene Dpyd (Figure 1A), which is a target of copper-mediated cell death (cuproptosis).[30]

Kyoto Encyclopedia of Genes and Genomes (KEGG), Gene Ontology (GO), Hallmark Analysis, and pathway relatedness further highlighted the distinct enrichment patterns in pathways associated with metabolism and cellular damage/tissue remodeling (Figures 1B–D and Supplemental Figures S1A–D, http://links.lww.com/HC9/B999). Metabolic pathways comprised the largest number of DEGs, including both cellular metabolism and xenobiotic detoxification mechanisms. Many of the significantly enriched pathways overlapped with metabolic pathways (Figure 1C and Supplemental Figure S1E, http://links.lww.com/HC9/B999). Detoxification signatures (cytochrome P450s, sulfotransferases, glutathione S transferases, and uracil glycotransferases) represented in retinol metabolism, chemical carcinogenesis-DNA adducts, steroid hormone biosynthesis, and xenobiotics via cytochrome P450 pathways were upregulated (Figure 1D and Supplemental Table S1B, http://links.lww.com/HC9/B995). Conversely, many DEGs were decreased within pathways encompassing lipid, glucose, and bile acid homeostasis (Fasn, Gck, Abcb11, Cyp8b1, Inmt, and Kynu) (Figure 1D and Supplemental Table S1B, http://links.lww.com/HC9/B995). *Atp7b*$^{-/-}$ mice showed increased collagen gene expression in the ECM–receptor interaction, protein digestion, and absorption pathways (Figure 1D and Supplemental Table S1B, http://links.lww.com/HC9/B995).

As expected from the more advanced pathology in these mice, changes in gene expression showed enrichment of the pathological network signatures. In silico analysis revealed enrichment of oncogenic and immune signatures, which agrees with recent studies linking copper excess with cancer, reviewed in Lutsenko et al[31] (Figures 1E, F; Supplemental Figures S1F, G, http://links.lww.com/HC9/B999; Supplemental Table S1C, http://links.lww.com/HC9/B995). Additionally, the DEG patterns in *Atp7b*$^{-/-}$ mice were consistent with exposure to chemicals and drugs known to mediate oxidative stress and detoxification pathways (Figure 1G;

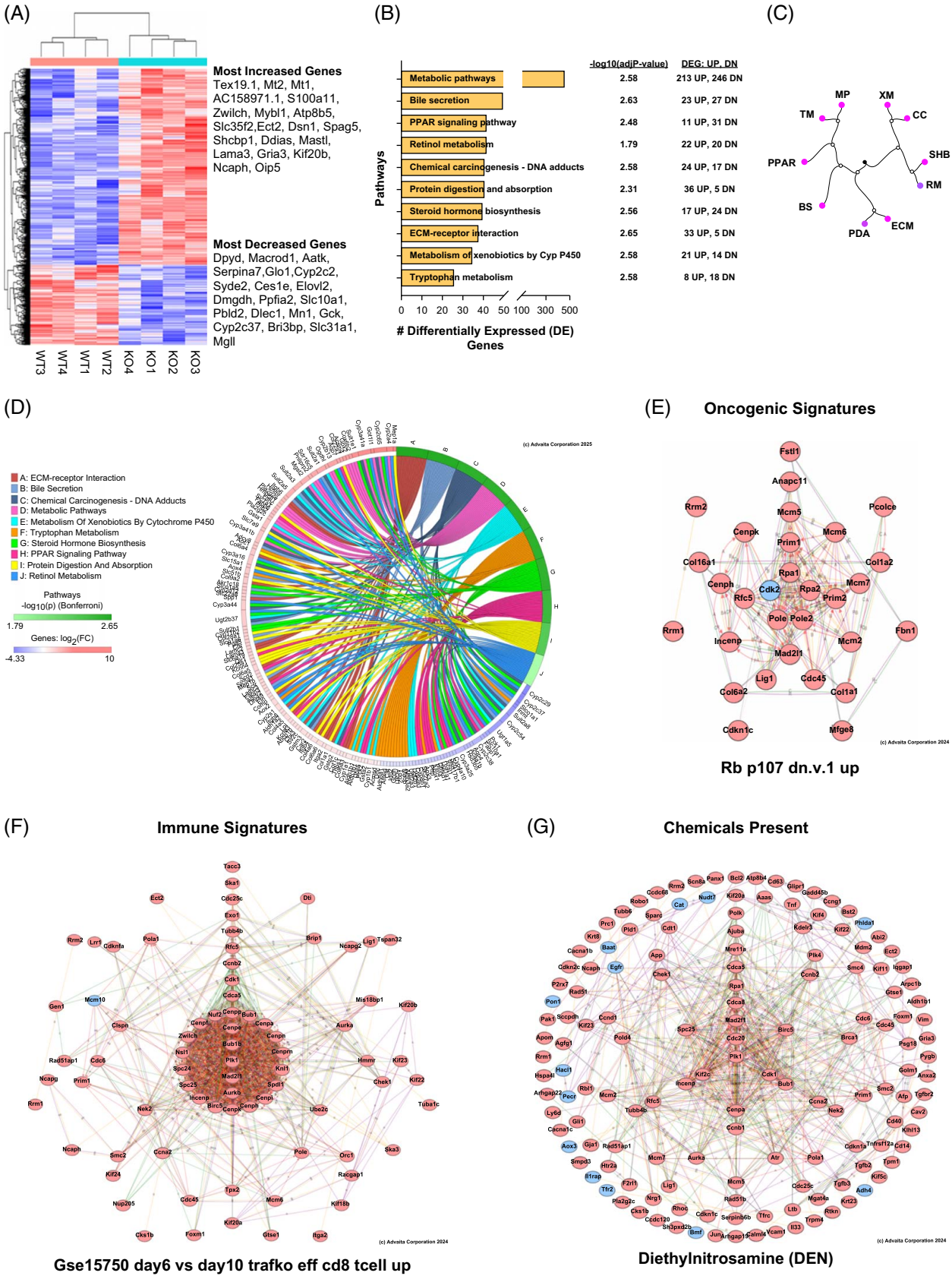

FIGURE 1 Transcriptomic profiles of *Atp7b*$^{-/-}$ mice. RNA-sequencing analysis of livers from 6-month-old male wild-type and *Atp7b*$^{-/-}$ mice. (A) Heat map of significantly changed (FDR < 0.05, FC < 1.5) genes. (B) Pathway analysis was determined using differentially expressed (DE) genes in *Atp7b*$^{-/-}$ versus WT mice. (C) Dendrogram depicting the relatedness of significantly enriched pathways. The node color corresponds to the significance of the *p* value for each pathway. Magenta circles represent the most significant results, and cyan represent lower significance.

Pathways are noted: MP, TM, PPAR, BS, PDA, ECM, RM, SHB, CC, and XM. (D) Chord diagram showing the overlap and uniqueness of the top 20 changed genes of significantly changed pathways. (E–G) Network analysis of hub genes (isolated nodes not shown) from the most significantly enriched data sets of oncogenic, immune, and chemicals present. Analyses for B–G and E–G were performed with Advaita iPathways software. Abbreviations: BS, bile secretion; CC, chemical carcinogenesis; ECM, extracellular matrix–receptor interaction; FC, fold change; FDR, false discovery rate; MP, molecular pathway; PDA, protein digestion and absorption; PPAR, PPAR signaling pathway; RM, retinal metabolism; SHB, steroid hydroxylase biosynthesis; TM, tryptophan metabolism; WT, wild type; XM, xenobiotic metabolism.

Supplemental Figure SG, http://links.lww.com/HC9/B999; Supplemental Table S1C, http://links.lww.com/HC9/B995). Several of these identified chemicals and drugs are well-known ligands for hepatic nuclear receptors, such as CAR and PXR [diethylnitrosamine (DEN), phenobarbital], PPARα (fatty acids, pirinixic acid), lithocholic acid (PXR, FXR), and pregnenolone carbonitrile (PXR), supporting a model of copper-mediated dysregulation of nuclear receptor signaling.

Overlap of publicly available single-cell RNA-sequencing analysis with DEGs of *Atp7b*$^{-/-}$ mice identified many non-liver "fetal" and "fibroblast" cell types, which suggests a reprogramming or dedifferentiation of liver cells in *Atp7b*$^{-/-}$ mice with moderate pathology (Figure 2A). In agreement with the derangement of liver cell types in *Atp7b*$^{-/-}$ mice, gene markers for stellate, bile duct, and Kupfer cell populations were increased, whereas gene markers for hepatoblasts and hepatocytes were mostly decreased (Figures 2A–F). These changes in enrichment patterns in *Atp7b*$^{-/-}$ mouse livers (Figure 2F) are similar to a ductular reaction gene signature in patients with alcohol-associated liver disease,[32] which is consistent with altered bile acid homeostasis and increased liver damage in *Atp7b*$^{-/-}$ livers.

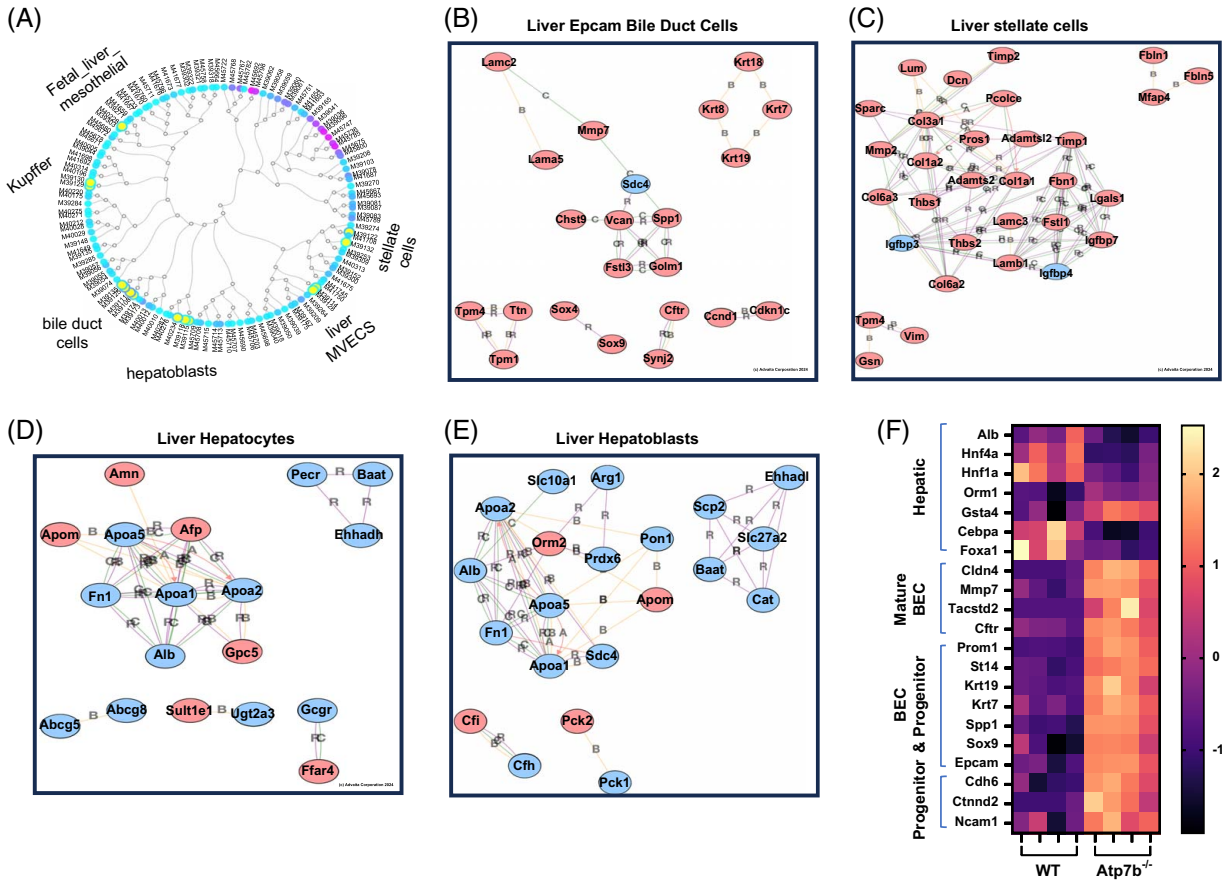

FIGURE 2 DEG changes in cell-type–specific markers in *Atp7b*$^{-/-}$ mice. Network analysis of RNA-sequencing data. (A) Dendrogram depicting the most prevalent cell types identified from RNA-sequencing transcriptome data of *Atp7b*$^{-/-}$ versus WT mice. Magenta circles represent the most significant results, and cyan represent lower significance. Yellow nodes represent liver cell types. (B–E) Network analysis showing interacting subnetworks (isolated nodes not shown) of data cell types representing enriched bile duct cells (B), stellate cells (C), hepatocytes (D), and hepatoblasts (E). (F) Heat map of significantly changed ($p < 0.05$) genes associated with progenitor, BEC, mature BEC, and hepatic cells in WT and Atp7b$^{-/-}$ mice. A–E were generated with Advaita iPathways software. Abbreviations: BEC, biliary epithelial cell; DEG, differential gene expression; MVECS, multivesicular endothelial cells; WT, wild type.

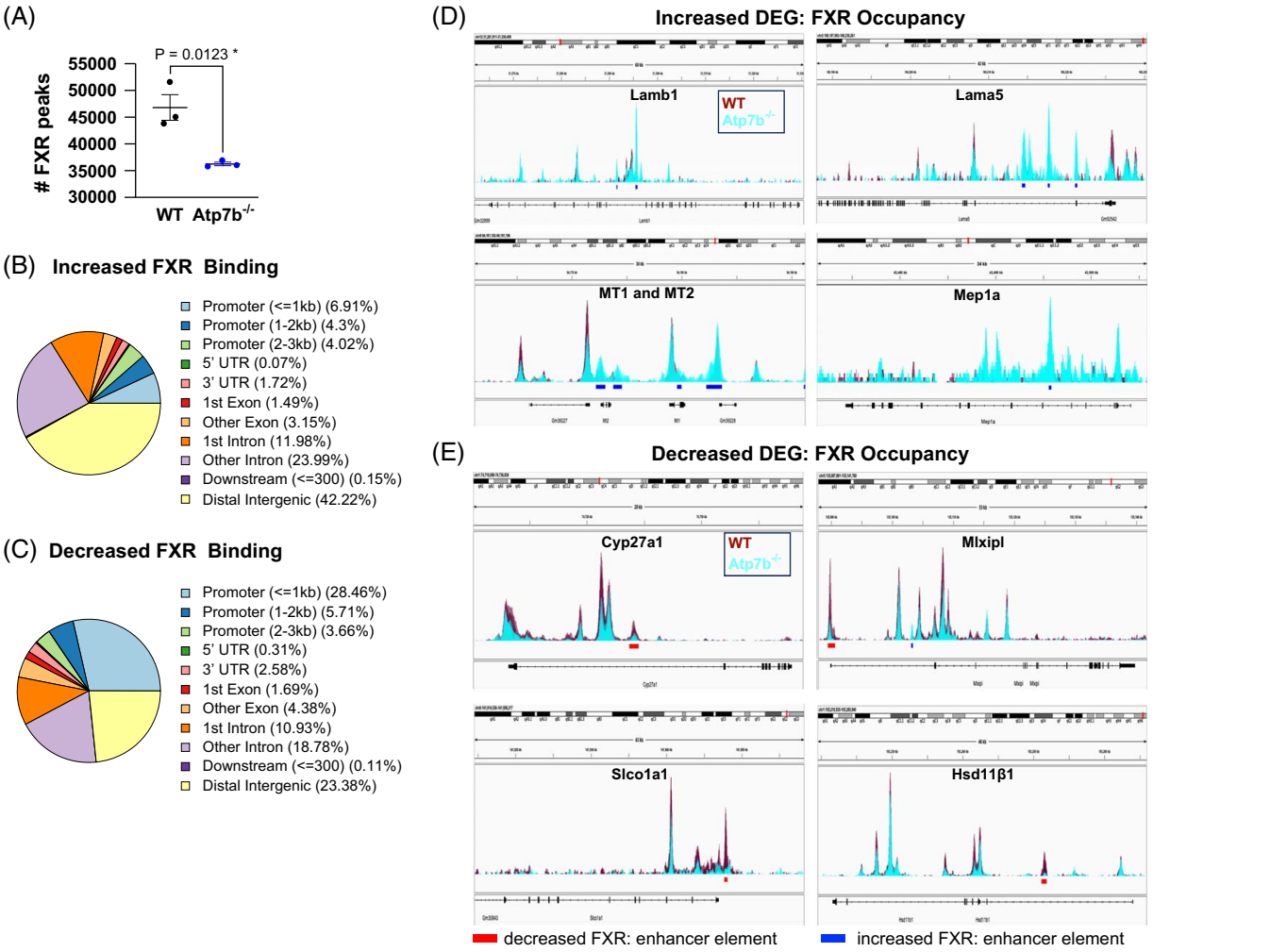
(A)
P = 0.0123 *
# FXR peaks
55000
50000
45000
40000
35000
30000
WT Atp7b-/-
(B) Increased FXR Binding
Promoter (<=1kb) (6.91%)
Promoter (1-2kb) (4.3%)
Promoter (2-3kb) (4.02%)
5' UTR (0.07%)
3' UTR (1.72%)
1st Exon (1.49%)
Other Exon (3.15%)
1st Intron (11.98%)
Other Intron (23.99%)
Downstream (<=300) (0.15%)
Distal Intergenic (42.22%)
(C) Decreased FXR Binding
Promoter (<=1kb) (28.46%)
Promoter (1-2kb) (5.71%)
Promoter (2-3kb) (3.66%)
5' UTR (0.31%)
3' UTR (2.58%)
1st Exon (1.69%)
Other Exon (4.38%)
1st Intron (10.93%)
Other Intron (18.78%)
Downstream (<=300) (0.11%)
Distal Intergenic (23.38%)
(D) Increased DEG: FXR Occupancy
Lamb1
WT
Atp7b-/-
Lama5
MT1 and MT2
Mep1a
(E) Decreased DEG: FXR Occupancy
Cyp27a1
WT
Atp7b-/-
Mlxipl
Slco1a1
Hsd11β1
decreased FXR: enhancer element
increased FXR: enhancer element

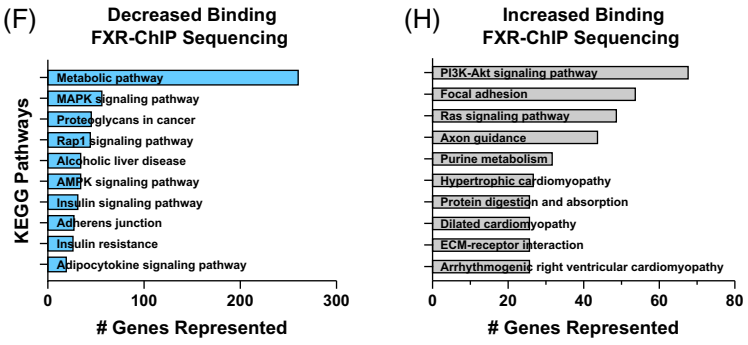
(F) Decreased Binding
FXR-ChIP Sequencing
KEGG Pathways
Metabolic pathway
MAPK signaling pathway
Proteoglycans in cancer
Rap1 signaling pathway
Alcoholic liver disease
AMPK signaling pathway
Insulin signaling pathway
Adherens junction
Insulin resistance
Adipocytokine signaling pathway
0
100
200
300
Genes Represented
(H) Increased Binding
FXR-ChIP Sequencing
PI3K-Akt signaling pathway
Focal adhesion
Ras signaling pathway
Axon guidance
Purine metabolism
Hypertrophic cardiomyopathy
Protein digestion and absorption
Dilated cardiomyopathy
ECM-receptor interaction
Arrhythmogenic right ventricular cardiomyopathy
0
20
40
60
80
Genes Represented

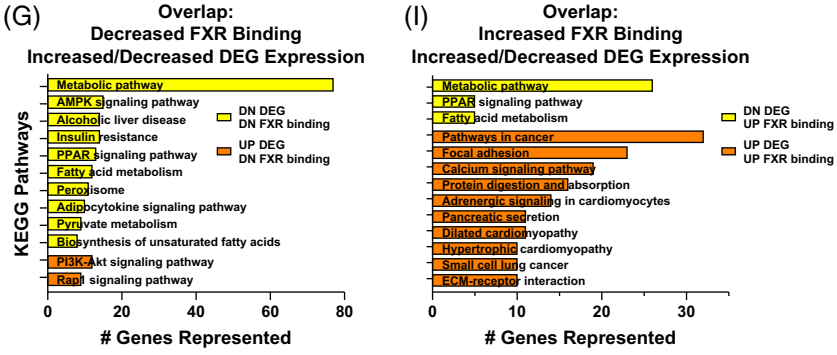
(G) Overlap:
Decreased FXR Binding
Increased/Decreased DEG Expression
KEGG Pathways
Metabolic pathway
AMPK signaling pathway
Alcoholic liver disease
Insulin resistance
PPAR signaling pathway
Fatty acid metabolism
Peroxisome
Adipocytokine signaling pathway
Pyruvate metabolism
Biosynthesis of unsaturated fatty acids
PI3K-Akt signaling pathway
Rap1 signaling pathway
DN DEG
DN FXR binding
UP DEG
DN FXR binding
0
20
40
60
80
Genes Represented
(I) Overlap:
Increased FXR Binding
Increased/Decreased DEG Expression
Metabolic pathway
PPAR signaling pathway
Fatty acid metabolism
Pathways in cancer
Focal adhesion
Calcium signaling pathway
Protein digestion and absorption
Adrenergic signaling in cardiomyocytes
Pancreatic secretion
Dilated cardiomyopathy
Hypertrophic cardiomyopathy
Small cell lung cancer
ECM-receptor interaction
DN DEG
UP FXR binding
UP DEG
UP FXR binding
0
10
20
30
Genes Represented

FIGURE 3 FXR occupancy and gene regulation are variable in parenchymal and non-parenchymal cells in *Atp7b*$^{-/-}$ mice. ChIP-seq was performed with FXR polyclonal antibody using chromatin from 6-month-old male WT and *Atp7b*$^{-/-}$ mice (n = 3 mice/group). (A) Total number of FXR-enriched peaks in WT and *Atp7b*$^{-/-}$ mice. (B, C) Differential FXR enrichment within *Atp7b*$^{-/-}$ cistrome was determined from the number of significantly changed peaks [*Atp7b*$^{-/-}$ vs. WT, fold change (FC) > 20%, adj. *p* value < 0.05]. (D, E) Representative FXR–ChIP-sequencing data generated with Integrative Genomics Viewer (IGV). FXR binding in WT (maroon) and *Atp7b*$^{-/-}$ (turquoise) overlap. *Atp7b*$^{-/-}$ mice with significant changes in FXR binding within enhancer elements are shown beneath peak tracings: decreased (red bars) and increased (blue bars). (F–I) Pathways represented in genes with increased and decreased FXR enrichment and significant changes in corresponding DEGs. (F–I) Generated with webgestalt.org. Abbreviations: DEGs, differentially expressed genes; FXR, farnesoid X receptor; KEGG, Kyoto Encyclopedia of Genes and Genomes; WT, wild type.

Differential patterns of FXR enrichment in *Atp7b*$^{-/-}$ mice

Previous studies showed decreased activity of several hepatic metabolic nuclear receptors, including FXR, in *Atp7b*$^{-/-}$ mice and patients with WD.[6,10,33] Building on these studies, we performed ChIP-seq experiments to determine the FXR cistrome in *Atp7b*$^{-/-}$ mice. PCA variable features showed differential segregation of peaks between WT and *Atp7b*$^{-/-}$ mice (Supplemental Figure S2A, http://links.lww.com/HC9/B999), and the total number of global hepatic FXR-binding events was reduced by 22% in *Atp7b*$^{-/-}$ versus WT mice ($p = 0.0123$) (Figure 3A). These findings confirm that FXR binding was decreased, but not abolished, in *Atp7b*$^{-/-}$ mice, consistent with prior studies.[6] Next, we determined the fold-change enrichment of FXR-bound peaks in *Atp7b*$^{-/-}$ versus WT mice (FC > 20%, adj. $p < 0.05$). Despite the decrease in FXR binding overall, the subset of peaks with significantly increased FXR occupancy (6793 peaks) was larger than the subset of peaks with decreased FXR enrichment (3605 peaks) (Supplemental Table S2, http://links.lww.com/HC9/C2), while the number of annotated genes with changes in FXR enrichment was similar (3972 genes with increased and 3292 with decreased FXR binding). Analysis of the genomic regions with either significantly increased or decreased FXR binding in *Atp7b*$^{-/-}$ mice revealed that increased FXR binding in *Atp7b*$^{-/-}$ mice was most prevalent in distal intergenic regions, whereas FXR occupancy in the proximal promoter regions (< 1 kb from transcription start site) was significantly lower in *Atp7b*$^{-/-}$ mice than WT mice (Figures 3B, C).

FXR occupancy within enhancer elements was also altered in *Atp7b*$^{-/-}$ versus WT mice (Figures 3D, E and Supplemental Figure S2C, http://links.lww.com/HC9/B999). To determine if these changes were associated with DEGs, peaks with significant changes in FXR enrichment and gene expression in *Atp7b*$^{-/-}$ versus WT mice were also examined for enhancer elements. The overlap of DEGs with increased expression and FXR occupancy in enhancer elements did not produce significant pathway enrichment (Supplemental Table S3, http://links.lww.com/HC9/B996). However, NAFLD, mTOR signaling, insulin signaling, AMP signaling, and insulin resistance were associated with downregulated gene expression and decreased FXR enhancer occupancy (Supplemental Figure S2C, http://links.lww.com/HC9/B999 and Supplemental Table S3, http://links.lww.com/HC9/B996). The mechanism for the differential FXR recruitment is unclear; however, decreased FXR occupancy within promoter and enhancer elements supports a model of impaired FXR activity resulting in decreased target gene expression in *Atp7b*$^{-/-}$ mice.

Further analysis of transcriptomic and cistromic data demonstrated that FXR occupancy status correlated with the transcriptome pathway analysis in *Atp7b*$^{-/-}$ mice. Pathway analysis of peaks with both decreased FXR binding and decreased DEG expression was dominated by hepatocyte-associated generic metabolic pathways as well as hepatocyte signaling (AMPK and PPAR) and disease (alcoholic liver disease and insulin resistance) processes (Figures 3F, G and Supplemental Table 3, http://links.lww.com/HC9/B996). In contrast, increased FXR binding and increased DEG expression were mapped to pathways outside of hepatocytes, including generic cancer, focal adhesion, and non-hepatocyte disease processes (Figures 3H, I, and Supplemental Table S3, http://links.lww.com/HC9/B996).

TABLE 1 FXR binding status in gene markers of significantly altered cell types in *Atp7b*$^{-/-}$ mouse livers

FXR binding	Hepatocytes (n = 169)	Bile ducts (n = 166)	MVECS (n = 135)	HSC (n = 110)	Kupffer cells (n = 22)
UP	13.0%	32.5%	36.0%	34.5%	22.7%
DOWN	23.1%	11.4%	14.1%	10.0%	0%
UP and DOWN	3.5%	4.2%	7.4%	4.5%	4.5%

Note: The percentage of FXR binding in representative genes of hepatocytes, bile ducts, microvascular endothelial cells (MVECS), hepatic stellate cells (HSC), and Kupffer cells (KC) is represented. Unique gene markers were identified with the iPathways Advaita software. Genes with overlapping expression among different cell types were excluded from analysis. The total number of changed marker genes is indicated below the cell type. The percentage of representative FXR binding was calculated (# gene markers with changed FXR binding/total # gene markers represented).
Abbreviations: FXR, farnesoid X receptor; MVECS, multivesicular endothelial cells.

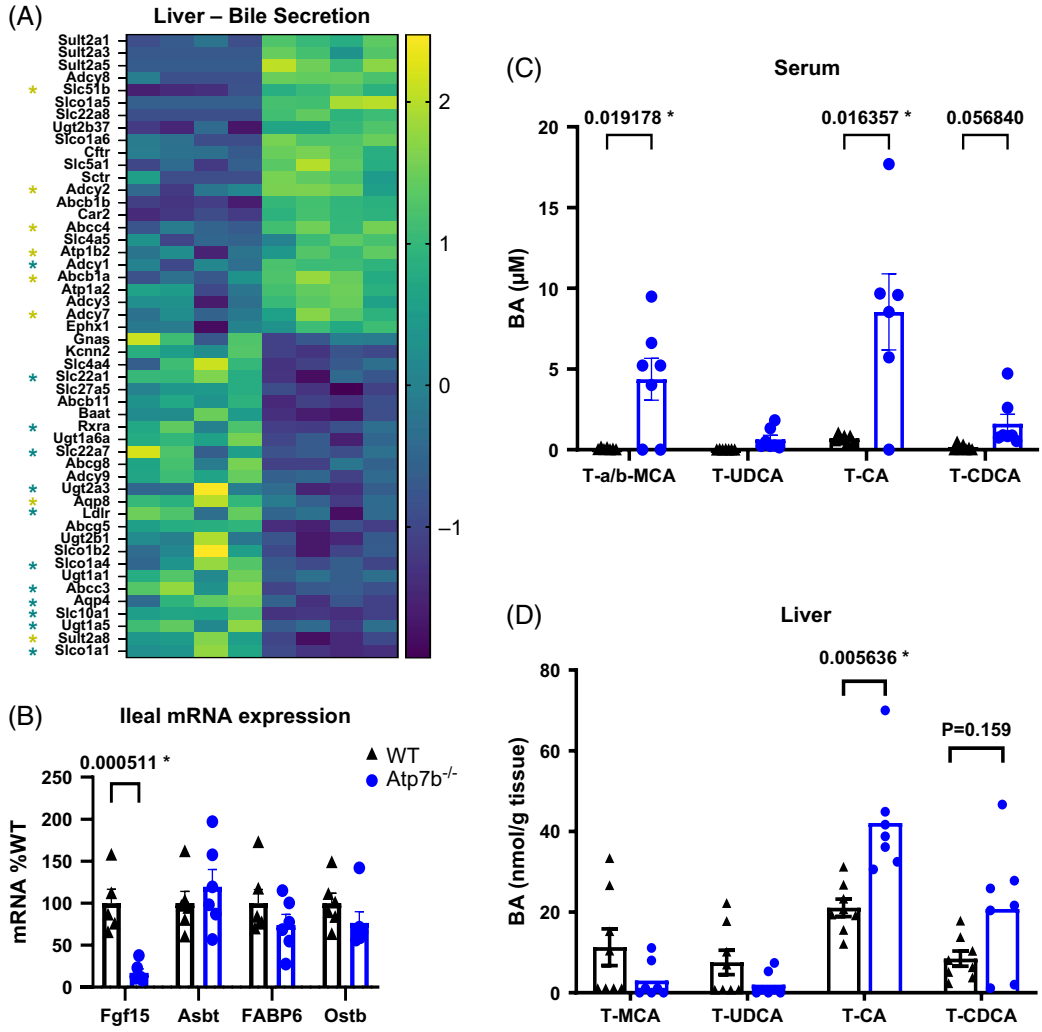

FIGURE 4 Alterations in bile acid metabolism in *Atp7b*$^{-/-}$ mice. (A) Heat map of significantly changed hepatic genes in the KEGG bile secretion pathway in 6-month-old Atp7b$^{-/-}$ versus WT mice (n = 4/group). Genes with differential FXR enrichment (*(lime green) increased, *(teal) decreased) are marked. (B) Ileal mRNA gene expression from 6-month-old WT and *Atp7b*$^{-/-}$ mice (n = 4–6/group). (C) Serum and (D) liver of 6–8-month-old WT and *Atp7b*$^{-/-}$ mice, n = 4–8 mice/group. Statistically significant differences were determined with the Student *t* test, indicated by *p* values < 0.05. Abbreviations: BA, bile acids; FXR, farnesoid X receptor; KEGG, Kyoto Encyclopedia of Genes and Genomes; WT, wild type.

These pathway analyses suggested cell-specific changes in FXR activity in *Atp7b*$^{-/-}$ mice consistent with the differential gene expression effects in parenchymal versus non-parenchymal cells described above (Figure 2). We therefore overlapped changes in cell-type–specific marker genes with FXR ChIP-seq data to assess differential patterns of FXR enrichment in parenchymal and non-parenchymal cells. In hepatocyte-specific DEGs, many more FXR binding sites showed decreased (23.1%) than increased (13.0%) occupancy (Table 1). Conversely, DEGs associated with bile ducts, multivesicular endothelial cells (MVECS), hepatic stellate cells (HSC), and Kupffer cells showed more increased (~30% enrichment) than decreased (~10%–15%) FXR binding (Table 1).

Altered bile acid homeostasis in *Atp7b*$^{-/-}$ mice and WD patients

Bile acid metabolism is tightly coordinated by hepatic and enterohepatic FXR activity. In agreement with this, FXR-binding status strongly correlated with alterations in expression of genes encoding hepatic transporters, sulfotransferases, bile acid synthetic enzymes, and UGTs, suggesting copper-mediated changes in bile flow and bile acid homeostasis (Figure 4A). Expression of the bile acid–FXR-regulated target gene Fgf15 decreased in the small intestine of *Atp7b*$^{-/-}$ mice, suggesting impairment of bile flow (Figure 4B). Given the alterations in FXR activity and expression of bile acid metabolism genes, we measured serum and hepatic bile acids in WT and

Atp7b$^{-/-}$ mice. Tauro-cholic acid (T-CA) and tauro-α/β-muricholic acid (T-MCA) bile acid concentrations were changed in *Atp7b*$^{-/-}$ mice: T-CA (serum, liver), T-MCA (serum), and tauro-chenodeoxycholic acid (T-CDCA) showed an upward trend, which was not statistically significant for their concentrations in either serum ($p = 0.056$) or liver ($p = 0.159$) (Figures 4C, D). Changes in hepatic (but not serum) bile acid composition were exacerbated in *Atp7b:FXR* double knockout (DKO$^{Atp7b:FXR}$) mice, indicating that *Atp7b*$^{-/-}$ mice retained partial FXR activity (Supplemental Figures S3A, B, http://links.lww.com/HC9/B999); however, neither bile salt exporter pump (Bsep) nor SHP mRNA expression was significantly decreased in DKO$^{Atp7b:FXR}$ mice relative to either *Atp7b*$^{-/-}$ or *FXR*$^{-/-}$ mice (Supplemental Figures S3C, D, http://links.lww.com/HC9/B999).

We obtained serum samples from adult male subjects (age range 25–65 yr old) without known liver or metabolic disease (healthy controls) and WD patients characterized as "liver," "neurological," or "mixed" disease (hepatic and neurological), as well as two newly diagnosed/early in treatment female WD patients with the "liver" phenotype. Due to the small size of the female cohort, we did not include these patients in the statistical analysis. Interestingly, the BMI of the healthy controls was slightly higher than that of WD patients (Table 2). Several WD patients with liver and mixed phenotypes had liver cirrhosis (7 out of 11, hepatic; 1 out of 3, mixed; Table 2). All male patients with WD in our study were on medical treatment (treatment-positive) (Supplemental Table S4, http://links.lww.com/HC9/B997). ALT, total bilirubin (TBILC), and direct bilirubin (DBILC) were significantly increased in WD: liver patients with cirrhosis (WD: liver + Cir) (Table 3). Total cholesterol and LDL serum concentrations were slightly decreased in the WD: liver + Cir group versus control patients (total cholesterol, $p = 0.215$; LDL, $p = 0.061$), similar to previous reports in WD patients with different serum lipid levels among the different WD phenotypes.[34] Non-cirrhotic WD: liver phenotype (WD: liver −Cir.) patients had increased TBILC but no other statistically significant changes in clinical chemistry. Aside from decreased serum triglyceride concentrations in the WD: mixed patients, the WD: mixed and WD: neuro patients did not have significant changes in markers of liver dysfunction or metabolism (Table 3). These findings are also congruent with those in *Atp7b*$^{-/-}$ mice and LEC rats, both of which develop liver but not neurological disease.[35] The small sample size of the female WD cohort prevented statistical analysis; however, their serum chemistries showed increased trends in markers of liver dysfunction (AST, ALT, and GGT; Table 3). Female patients with WD presented with liver symptoms and were in the early phases of treatment, and their testing and symptoms would be expected to normalize with longer WD-targeted therapies. The small sample size in this study may have obscured significant changes in the WD phenotypes. Future studies will require increased sample sizes for all groups, especially in female control and WD populations.

Total bile acid levels in the serum of WD patients were not significantly increased when compared to healthy controls (Supplemental Figures S4A–D, http://links.lww.com/HC9/B999). Despite an upward trend in both total and conjugated bile acids in WD: liver + Cir. compared to healthy patients, these changes were not statistically significant (Supplemental Figures S4B, C, http://links.lww.com/HC9/B999). Comparison of bile acid profiles in WD patients with "liver," "neurological," or "mixed" disease versus healthy controls (Figures 5A–G) revealed increased T-CA and glyco-CA (GCA) in WD: liver +Cir. versus healthy controls (Figures 5B, E). T-CDCA and G-CDCA were not statistically different in WD: liver +Cir. relative to healthy controls (T-CDCA, $p = 0.1366$ and G-CDCA, $p = 0.1203$), but demonstrated an increasing trend similar to that of T-CA and G-CA species. The female cohort lacked sufficient sampling numbers for statistical analysis; however, the serum bile acid

TABLE 2 General characteristics of control and Wilson disease patients

Disease	Cirrhosis (+)	Cirrhosis (−)	Age	BMI
Control	0	17	53 ± 1.94	29.9 ± 1.69
WD: Liver (all)	7	4	51.4 ± 3.53	27.0 ± 1.08
WD: Liver (−Cirrhosis)	—	4	48.5 ± 5.01	25.1 ± 0.68
WD: Liver (+Cirrhosis)	7	—	53.9 ± 5.12	28.7 ± 1.73
WD: Neuro.	0	3	55.2 ± 2.98	27.7 ± 0.84
WD: Mixed	2	1	42.7 ± 10.14	27.9 ± 2.42
Female WD: Liver	0	2	34 ± 4.34	24.64 ± 1.02

Abbreviations: BMI, body mass index; WD, Wilson disease

The Mean +/- the SEM are shown for each group.

Note: Patients were grouped according to phenotype of WD presentation. Liver—patients presenting with only liver symptoms, which is broken down further into liver – cirrhosis and liver +cirrhosis; neurological (neuro.)—patients with only neurological symptoms; mixed—both liver and neurological symptoms. The 2 female patients in the study presented with liver symptoms.

TABLE 3 Clinical chemistry panels of control and Wilson disease patients

	Con., n = 17	WD: liver−Cir., n = 4	WD: liver+Cir., n = 7	WD: neuro, n = 3	WD: mixed, n = 3	WD: liver female, n = 2
AST	21.7 ± 1.0	33.1 ± 9.9	25.5 ± 2.4	33.0 ± 7.3	23 ± 2.5	42.9 ± 11.9
ALT	23.8 ± 1.7	54.8 ± 26.3	*34.7 ± 4.2[a], p = 0.015*	47.7 ± 15.4	40.4 ± 11.8	67.8 ± 29.6
ALP	73 ± 4.3	78.6 ± 12.8	84.2 ± 5.7	101 ± 24.6	81.5 ± 12.2	63.7 ± 11.3
LDH	159 ± 7.4	153 ± 2.7	147 ± 18.0	133 ± 3.3	133 ± 16.6	157 ± 4.7
GGT	33.9 ± 8.9	24.6 ± 3.8	32.70 ± 4.4	50.6 ± 18.4	27.2 ± 4.9	46.8 ± 16
DBR	0.11 ± 0.008	0.14 ± 0.02	*0.21 ± 0.043[a], p < 0.0001*	0.107 ± 0.007	0.200 ± 0.056	0.15 ± 0.05
TBR	0.41 ± 0.03	*0.58 ± 0.057[a], p = 0.009*	*0.84 ± 0.165[a], p < 0.0001*	0.47 ± 0.039	0.80 ± 0.35	0.5 ± 0.10
Chol	195.0 ± 10.5	224.0 ± 17.7	173.00 ± 11.0	188 ± 23.1	173 ± 18.4	209 ± 24.5
HDL	48.1 ± 3.2	50.6 ± 6.95	43.40 ± 4.89	42.9 ± 6.68	46.4 ± 8.3	57.9 ± 5.1
LDL	104.0 ± 9.0	117.0 ± 11.2	79.10 ± 5.41	99.6 ± 17.3	95.4 ± 10.3	104 ± 25.9
TG	149.0 ± 16.0	206.0 ± 87.6	142.00 ± 15.6	224 ± 91.3	*86.0 ± 9.19[a], p = 0.005*	143 ± 21.1
Total protein	7.5 ± 0.17	7.7 ± 0.47	7.071 ± 0.39	7.88 ± 0.22	6.77 ± 0.52	7.3 ± 0.2
Albumin	4.7 ± 0.097	4.8 ± 0.149	4.96 ± 0.16	4.76 ± 0.87	4.73 ± 0.12	4.75 ± 0.15

Note: Clinical chemistry findings are presented by group.
[a]$p < 0.05$ as determined with the Student *t* test versus the control (con.) group.
Abbreviations: Cir., cirrhosis; con. control; Chol, cholesterol; DBR, direct bilirubin; LDH, lactate dehydrogenase; TBR: total bilirubin; TG: triglycerides; WD, Wilson disease.

concentrations were similar to those of the male control samples (Figure 5G). As expected, glycine-conjugated bile acids were the most abundant conjugated species in both control (89.5%) and WD: Liver patients (77.4%); however, taurine-conjugated bile acids were more prevalent in WD: liver patients (10.5% in control and 25.4% in WD: liver patients), especially in WD: liver +Cir. group (Figures 5H, I). In contrast, changes in amino acid conjugation were not found in WD: neuro or WD: mixed patients, suggesting that speciation differences are specific to WD patients with liver dysfunction.

Fatty liver is a common clinical finding in patients with WD; therefore, we compared serum bile acids in patients with WD and MASLD. The MASLD cohort included 3 of 12 patients with liver cirrhosis; therefore, we analyzed whether differences were observed in the non-cirrhotic versus cirrhotic MASLD patients. The MASLD + cirrhosis group showed the most significant changes relative to the healthy control group, including slight increases in ALP, DBILC, and TBILC (Supplemental Table S5, http://links.lww.com/HC9/B998). Like WD: Liver + Cir, cirrhotic MASLD patients had the most significant changes in bile acid composition compared to control patients (Supplemental Figures S5A–F, http://links.lww.com/HC9/B999). The bile acid profiles of cirrhotic WD and MASLD patients were similar between the two groups (Supplemental Figure 5G, http://links.lww.com/HC9/B999); however, there were no significant differences between the percentages of taurine-conjugated and glycine-conjugated species in the MASLD and control groups.

DISCUSSION

Copper is a well-studied essential trace element that is necessary for many biological processes, including cellular metabolism, energy production, iron metabolism, blood clotting, and signal transduction (reviewed in Lutsenko et al[31]). Disruption of cellular copper homeostasis occurs in WD, a rare genetic disorder that most often affects the liver and brain. WD patients present with either neurological, hepatic, or mixed phenotypic presentation, which may preclude a timely diagnosis of WD. Copper is well known to mediate redox chemistry, and copper imbalance has been linked to cancer (cuproptosis) and metabolic dysfunction. Herein, we extend previous findings of nuclear receptor dysregulation in the liver, with a specific focus on FXR activity and congruent changes in bile acid physiology.

Previous studies demonstrated that presymptomatic *Atp7b*$^{-/-}$ mice had increased gene expression for cell cycle pathways and markers of cell proliferation, whereas those for lipid metabolism pathways were decreased,[3] suggesting that copper-mediated oxidative stress was not the only factor that initiated liver injury in WD. The progressive nature of untreated WD was evidenced by extensive changes in DEGs, particularly the divergent patterns of enrichment associated with cellular damage and metabolism. Accumulation of markers for bile duct cells, ECM-related mechanisms, and CXCR4 expression, along with decreased hepatocyte gene signatures, suggested a hepatocyte dedifferentiation phenotype in untreated *Atp7b*$^{-/-}$ mice over time and is supported by the

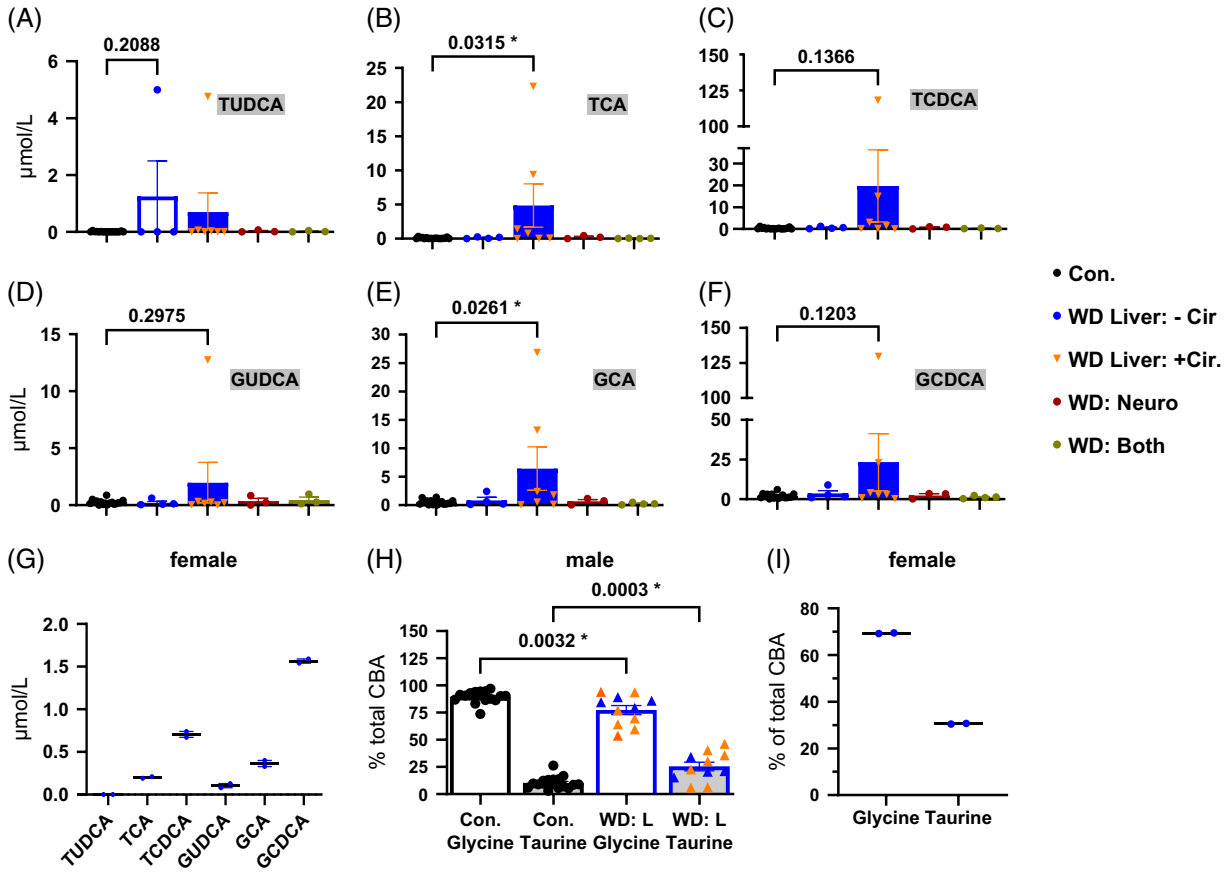

FIGURE 5 Alterations in bile acid metabolism in Wilson disease patients. (A–F) Bile acids were quantified from the serum of non-fasted healthy males (control) and WD treatment-positive males and females (G) aged 25–65 (Baylor College of Medicine and Wilson Disease Registry). Control (n = 17) and WD patients with liver symptoms (non-cirrhotic, L −Cir, n = 4; cirrhotic, L +Cir, n = 7), neurological (N, n = 3), and both (liver and neurological symptoms, n = 3). (H, I) % of conjugated bile acids (CBA) in control and WD (liver) male and female patients. Statistically significant differences were determined using one-way ANOVA followed by the Dunnett multiple comparison test. Statistically significant p values are indicated by $p < 0.05$. Abbreviations: GCA, glycocholic acid; GCDCA, glycochenodeoxycholic acid; GUDCA, glycoursodeoxycholic acid; TCA, taurocholic acid; TCDCA, taurochenodeoxycholic acid; TUDCA, tauroursodeoxycholic acid; WD, Wilson disease.

discordance of FXR-binding in parenchymal versus non-parenchymal cells in *Atp7b*$^{-/-}$ mice. Previous studies have reported shared transcriptomic signatures between WD and HCC patients, as well as for cholangiocarcinoma development in WD patients.[36–38] *Atp7b*$^{-/-}$ mice exhibited gene signatures similar to those of alcohol-associated hepatitis patients with ductular reaction[32] and patients with HCC that had an "onco-fetal" reprogramming of endothelial cells.[39] Despite changes in hepatocellular signaling, there is no consensus on whether WD patients have an elevated risk for HCC.

Gene enrichment within members of the cytochrome P450 (P450) family was identified in *Atp7b*$^{-/-}$ mice. P450s are heme-containing monooxygenases critical for many aspects of metabolism, including cellular metabolism and the biotransformation of metabolites. Although P450s are critical for the detoxification of the liver, reactive oxygen species may be generated during P450 catalysis of oxidative reactions.[40] *Atp7b*$^{-/-}$ mice showed increased expression of P450s related to xenobiotic metabolism (Cyp2b10 and Cyp2b13); however, P450s involved in bile acid metabolism (Cyp27a1 and Cyp8b1) and arachidonic acid metabolism (Cyp2c family and Cyp4a10) were significantly decreased. Hepatic P450 gene expression is regulated by nuclear receptors (CAR, PXR, FXR, LXR, and PPARα),[41] and pathway and network analyses identified CAR, PXR, and PPARα regulatory signatures in *Atp7b*$^{-/-}$ mice. These nuclear receptors, along with FXR, share regulatory elements across the cistrome, which may explain, at least partly, the redundancy of pathway enrichment in *Atp7b*$^{-/-}$ mice. This redundancy also complicates the identification of and therapeutic targeting of a specific nuclear receptor.

Patients with WD and animal models with copper-induced liver injury have reduced nuclear receptor activity and target gene expression. In vitro binding studies with estrogen receptor alpha (ERα) and FXR point to the direct copper-mediated disruption of nuclear receptor binding with response elements on target gene promoters.[3–6] The overall number of FXR peaks was reduced in *Atp7b*$^{-/-}$ versus WT mice; however, we unexpectedly found a

substantial subset of peaks with a statistically significant increase in FXR occupancy. Increased FXR binding is expected due to the increased levels of hepatic bile acids and was observed in some positive FXR hepatocyte targets (Figure 4A), but it is unclear why these genes were apparently able to overcome the general decrease in FXR activity. Interestingly, changes in FXR-occupancy varied by cell type: FXR-binding was primarily reduced in hepatocyte-specific DEGs, whereas FXR-occupancy was generally increased in DEGs associated with non-parenchymal cells of *Atp7b*$^{-/-}$ mice. Although previous results suggest that copper levels in younger/presymptomatic *Atp7b*$^{-/-}$ mice are increased in both parenchymal and non-parenchymal cells,[42] it remains possible that the increase in copper levels could be higher in *Atp7b*$^{-/-}$ hepatocytes than in non-hepatocytes and further studies will clarify copper-mediated effects in parenchymal and non-parenchymal cells.

FXR enrichment primarily occurred in gene bodies, whereas peaks with a significant reduction in FXR binding were located within the promoter regions. Further investigation of genes with a significant increase in FXR enrichment primarily mapped to proliferative pathways, whereas genes with decreased FXR binding mapped to metabolic pathways. We postulate that changes in chromatin structure or accessibility are altered by excess copper and affect FXR access to FXR response elements on the promoters of target genes.

Decreased FXR-occupancy mapped to enhancer elements of genes associated with metabolic processes, and FXR-mediated regulation of the gene expression of enhancer elements has been previously described.[43,44] Gene expression of Foxa2, a recently described pioneer factor that promotes ligand-dependent activation of FXR, was decreased in *Atp7b*$^{-/-}$ versus WT mice (Supplemental Table 1A, http://links.lww.com/HC9/B995). The decrease in Foxa2 gene expression may reinforce the negative impact of zinc displacement by copper on FXR binding within promoters and enhancers, despite an increase in serum bile acids in *Atp7b*$^{-/-}$ mice. In addition, epigenomic studies in WD patients identified regions of hypermethylation in liver-specific enhancer regions that were adjacent to RXR-binding motifs.[45]

The dysregulation of FXR recruitment to metabolic target genes, particularly genes required for maintenance of bile acid metabolism, supports previous findings of altered bile acid synthesis and metabolism in *Atp7b*$^{-/-}$ mice.[6] Our current study using older *Atp7b*$^{-/-}$ mice demonstrated changes in bile acid speciation in serum and hepatic bile acids compared to age-matched WT mice. Both hydrophilic (T-MCA) and hydrophobic (T-CA) levels were increased in the serum; however, only tricarboxylic acid levels were significantly increased in the liver. Given the retention of FXR binding in the cistrome, we investigated whether complete loss of FXR expression exacerbated changes in the bile acid pool of *Atp7b*$^{-/-}$ mice. Despite no significant differences between Bsep and SHP mRNA in *Atp7b*$^{-/-}$ versus DKO$^{Atp7b:\ FXR}$, alterations in hepatic bile acid composition were exacerbated in DKO$^{Atp7b:FXR}$, indicating that *Atp7b*$^{-/-}$ mice retained partial FXR activity. It is likely that copper dysregulation in enterocytes impacts bile acid metabolism because the liver–gut axis plays an integral role in bile acid homeostasis. Indeed, Fgf15 mRNA expression was decreased in the small intestine of *Atp7b*$^{-/-}$ mice, indicating a cholestatic-like phenotype in *Atp7b*$^{-/-}$ mice. Other studies have shown alterations in the gut microbiome and intestinal lipid absorption in *Atp7b*$^{-/-}$ mouse models.[46,47] Taken together, it is likely that the liver–gut axis regulation of bile acid homeostasis is disrupted in *Atp7b*$^{-/-}$ mice.

Clinical diagnosis and identification of novel therapeutic targets for WD treatment are complicated by the heterogeneous presentation of the disease. Efforts to identify unique metabolic signatures in WD clinical subtypes suggest unique metabolic profiles among the different clinical presentations.[7] Previous studies demonstrated increases in GCA and GUDCA in WD patients with neurological and hepatic symptoms relative to healthy control subjects.[48] In the present study, changes in bile acid composition were most associated with liver cirrhosis in both WD and MASLD patients, which agrees with a generally worse liver prognosis. WD patients with hepatic symptoms had an increase in the percentage of taurine-conjugated bile acids relative to healthy control patients, which contrasted with our MASLD cohort. Other liver disorders, such as alcoholic liver cirrhosis and hepatitis C, also exhibited increased levels of serum taurine-conjugated bile acids.[49,50] In hepatitis C patients, an increase in taurine-conjugated bile acids was linked to increases in the G-protein-coupled bile acid receptor S1PR2 and inflammation.[50] Fatty liver is often associated with WD, but the unique amino acid conjugation findings in WD:Liver group suggest that changes in bile acid conjugation have specific copper-driven changes in bile acid metabolism. It is plausible that increased glutathione synthesis decreases the available glycine pool in WD patients.

Substantial transcriptomic data in WD animal models identify early changes in genes that regulate bile acid synthesis, hepatic uptake, and biliary secretion prior to significant hepatocellular changes. Identification of a link between bile acid dysregulation and metabolic homeostasis and metabolic composition in WD patients is less straightforward, not only because of the array of symptoms but also because of comorbidities (such as diabetes and cancer) and lifestyle influences (diet, activity/exercise, etc.). It is unclear whether observed gene signatures at later disease stages are primarily the result of copper-mediated hepatic redox stress and nuclear receptor dysregulation or whether secondary changes in metabolic intermediates contribute to the pathology observed in WD.

Our studies provide new data that demonstrate changes in bile acid metabolism in *Atp7b*$^{-/-}$ mice and WD patients, as well as unexpected complexity in FXR-binding in the hepatic cistrome of *Atp7b*$^{-/-}$ mice. Recent

studies in our lab, as well as others, have identified changes in serum metabolites that are unique to *Atp7b*$^{-/-}$ mice[10] and WD patients.[7] The relationship between these observed metabolic changes and changes in copper-mediated pathology is not well understood, although hydrophobic bile acids (cholic acids) are known to have hepatocellular toxic effects. Future studies will aid in the identification of therapeutics that may selectively modify hepatocellular metabolism to alleviate copper-mediated liver toxicity in WD.

DATA AVAILABILITY STATEMENT

RNA and ChIP Sequencing raw data are located in GEO (GSE287020 and GSE286956).

AUTHOR CONTRIBUTIONS

Clavia Ruth Wooton-Kee designed, collected/analyzed data, and wrote the paper; Hari K. Yalamanchili analyzed RNA and ChIP-Seq data and assisted with figures; Islam Mohamed, Manal Hassan, and Prasun Jalal acquired patient samples; Ayse K. Coskun and Michael L. Schilsky acquired Wilson disease samples and edited the manuscript; Vasanta Putluri, Nagireddy Putluri, Kenneth D.R. Setchell, and Monica Narvaez Rivas analyzed bile acids in humans and mice; David D. Moore assisted with experimental design and edited the paper. All authors read and provided edits/suggestions for the manuscript.

FUNDING INFORMATION

Michael L. Schilsky receives grant support from the Wilson Disease Association, Orphalan, Vivet Therapeutics, and NIH R01 GR124795. Clavia Ruth Wooton-Kee received funding from NIH K01 DK111716-01, R01DK129579-01A1, and USDA/ARS 3092-51000-062-03S. Hari K. Yalamanchili received funding from USDA/ARS 58-3092-0-001 and Duncan NRI Zoghbi Scholar Award.

CONFLICTS OF INTEREST

Kenneth D.R. Setchell holds equity in Asklepion Pharmaceuticals, Baltimore, and Aliveris srl, Italy, and is a consultant to Mirum Pharmaceuticals, California. Michael L. Schilsky receives grant support from the Wilson Disease Association, Orphalan, Vivet Therapeutics and is a consultant to Arbomed, DepYmed, and Orphalan. The remaining authors have no conflicts to report.

DISCLOSURES

Kenneth D.R. Setchell holds equity in Asklepion Pharmaceuticals, Baltimore, and Aliveris srl, Italy, and is a consultant to Mirum Pharmaceuticals, California. Michael L. Schilsky receives grant support from the Wilson Disease Association, Orphalan, Vivet Therapeutics and is a consultant to Arbomed, DepYmed, and Orphalan.

ORCID

Clavia Ruth Wooton-Kee https://orcid.org/0000–0003–4485–0747
Hari K. Yalamanchili https://orcid.org/0000–0001–9892–3054
Ayse K. Coskun https://orcid.org/0000–0002–9339–3418
Nagireddy Putluri https://orcid.org/0000–0003–4488–7400
Prasun Jalal https://orcid.org/0000–0001–5353–2324
Michael L. Schilsky https://orcid.org/0000–0001–9043–0554
David D. Moore https://orcid.org/0000–0002–5151–9748

REFERENCES

1. Sandahl TD, Laursen TL, Munk DE, Vilstrup H, Weiss KH, Ott P. The prevalence of Wilson's disease: An update. Hepatology. 2020;71:722–32.
2. Weiss KH, Schilsky M. Wilson disease. In: Adam MP, Mirzaa GM, Pagon RA, et al., eds. GeneReviews((R)). Seattle, WA: University of Washington, Seattle; 1993.
3. Wooton-Kee CR. Therapeutic implications of impaired nuclear receptor function and dysregulated metabolism in Wilson's disease. Pharmacol Ther. 2023;251:108529.
4. Deegan BJ, Bona AM, Bhat V, Mikles DC, McDonald CB, Seldeen KL, et al. Structural and thermodynamic consequences of the replacement of zinc with environmental metals on estrogen receptor alpha-DNA interactions. J Mol Recognit. 2011;24:1007–17.
5. Predki PF, Sarkar B. Effect of replacement of "zinc finger" zinc on estrogen receptor DNA interactions. J Biol Chem. 1992;267:5842–6.
6. Wooton-Kee CR, Jain AK, Wagner M, Grusak MA, Finegold MJ, Lutsenko S, et al. Elevated copper impairs hepatic nuclear receptor function in Wilson's disease. J Clin Invest. 2015;125:3449–60.
7. Sarode GV, Kim K, Kieffer DA, Shibata NM, Litwin T, Czlonkowska A, et al. Metabolomics profiles of patients with Wilson disease reveal a distinct metabolic signature. Metabolomics. 2019;15:43.
8. Johansen K, Gregersen G. Glucose intolerance in Wilson's disease. Normalization after treatment with penicillamine. Arch Intern Med. 1972;129:587–90.
9. Xu J, Jiang H, Li J, Cheng KK, Dong J, Chen Z. 1H NMR-based metabolomics investigation of copper-laden rat: A model of Wilson's disease. PLoS One. 2015;10:e0119654.
10. Wooton-Kee CR, Robertson M, Zhou Y, Dong B, Sun Z, Kim KH, et al. Metabolic dysregulation in the Atp7b (−/−) Wilson's disease mouse model. Proc Natl Acad Sci USA. 2020;117:2076–83.
11. Hamilton JP, Koganti L, Muchenditsi A, Pendyala VS, Huso D, Hankin J, et al. Activation of LXR/RXR pathway ameliorates liver disease in Atp7b (Wilson disease) mice. Hepatology. 2016;63:1828–41.
12. Huster D, Purnat TD, Burkhead JL, Ralle M, Fiehn O, Stuckert F, et al. High copper selectively alters lipid metabolism and cell cycle machinery in the mouse model of Wilson disease. J Biol Chem. 2007;282:8343–55.
13. Muchenditsi A, Talbot CC Jr, Gottlieb A, Yang H, Kang B, Boronina T, et al. Systemic deletion of Atp7b modifies the hepatocytes' response to copper overload in the mouse models of Wilson disease. Sci Rep. 2021;11:5659.
14. Gottlieb A, Dev S, DeVine L, Gabrielson KL, Cole RN, Hamilton JP, et al. Hepatic steatosis in the mouse model of Wilson disease coincides with a muted inflammatory response. Am J Pathol. 2022;192:146–59.

15. Levy E, Brunet S, Alvarez F, Seidman E, Bouchard G, Escobar E, et al. Abnormal hepatobiliary and circulating lipid metabolism in the Long-Evans Cinnamon rat model of Wilson's disease. Life Sci. 2007;80:1472–83.
16. Somm E, Jornayvaz FR. Fibroblast growth factor 15/19: From basic functions to therapeutic perspectives. Endocr Rev. 2018; 39:960–89.
17. Panzitt K, Zollner G, Marschall HU, Wagner M. Recent advances on FXR-targeting therapeutics. Mol Cell Endocrinol. 2022;552: 111678.
18. Chiang JYL, Ferrell JM. Discovery of farnesoid X receptor and its role in bile acid metabolism. Mol Cell Endocrinol. 2022;548: 111618.
19. Chiang JYL. Bile acids: Regulation of synthesis. J Lipid Res. 2009;50:1955–66.
20. Zhang M, Chiang JYL. Transcriptional regulation of the human sterol 12alpha-hydroxylase gene (CYP8B1): Roles of heaptocyte nuclear factor 4alpha in mediating bile acid repression. J Biol Chem. 2001;276:41690–9.
21. Kong B, Wang L, Chiang JYL, Zhang Y, Klaassen CD, Guo GL. Mechanism of tissue-specific farnesoid X receptor in suppressing the expression of genes in bile-acid synthesis in mice. Hepatology. 2012;56:1034–43.
22. Anakk S, Watanabe M, Ochsner SA, McKenna NJ, Finegold MJ, Moore DD. Combined deletion of Fxr and Shp in mice induces Cyp17a1 and results in juvenile onset cholestasis. J Clin Invest. 2011;121:86–95.
23. Committee for the Update of the Guide for the Care and Use of Laboratory Animals, Institute for Laboratory Animal Research, Division on Earth and Life Studies, National Research Council of the National Academies. Guide for the Care and Use of Laboratory Animals, 8th ed. Washington, DC: The National Academies Press; 2011.
24. Love MI, Huber W, Anders S. Moderated estimation of fold change and dispersion for RNA-seq data with DESeq2. Genome Biol. 2014;15:550.
25. Zhang Y, Liu T, Meyer CA, Eeckhoute J, Johnson DS, Bernstein BE, et al. Model-based analysis of ChIP-Seq (MACS). Genome Biol. 2008;9:R137.
26. Wang Q, Li M, Wu T, Zhan L, Li L, Chen M, et al. Exploring epigenomic datasets by ChIPseeker. Curr Protoc. 2022;2:e585.
27. Gao T, Qian J. EnhancerAtlas 2.0: an updated resource with enhancer annotation in 586 tissue/cell types across nine species. Nucleic Acids Res. 2020;48(D1):D58–64.
28. St John-Williams L, Mahmoudiandehkordi S, Arnold M, Massaro T, Blach C, Kastenmüller G, et al. Bile acids targeted metabolomics and medication classification data in the ADNI1 and ADNIGO/2 cohorts. Sci Data. 2019;6:212.
29. Rosen R, Lurie M, Kane M, DiFilippo C, Cohen A, Freiberger D, et al. Risk factors for bile aspiration and its impact on clinical outcomes. Clin Transl Gastroenterol. 2021;12:e00434.
30. Tsvetkov P, Coy S, Petrova B, Dreishpoon M, Verma A, Abdusamad M, et al. Copper induces cell death by targeting lipoylated TCA cycle proteins. Science. 2022;375:1254–61.
31. Lutsenko S, Roy S, Tsvetkov P. Mammalian copper homeostasis: Physiologic roles and molecular mechanisms. Physiol Rev. 2025;105:441–91.
32. Aguilar-Bravo B, Ariño S, Blaya D, Pose E, Martinez García de la Torre RA, Latasa MU, et al. Hepatocyte dedifferentiation profiling in alcohol-related liver disease identifies CXCR4 as a driver of cell reprogramming. J Hepatol. 2023;79:728–40.
33. Wu X, Chien H, van Wolferen ME, Kruitwagen HS, Oosterhoff LA, Penning LC. Reduced FXR target gene expression in copper-laden livers of COMMD1-deficient dogs. Vet Sci. 2019;6:78.
34. Seessle J, Gohdes A, Gotthardt DN, Pfeiffenberger J, Eckert N, Stremmel W, et al. Alterations of lipid metabolism in Wilson disease. Lipids Health Dis. 2011;10:83.
35. Kim KH, Wooton-Kee CR. Editorial for the MCE special issue on "FXR and metabolism". Mol Cell Endocrinol. 2023;565:111889.
36. Pfeiffenberger J, Mogler C, Gotthardt DN, Schulze-Bergkamen H, Litwin T, Reuner U, et al. Hepatobiliary malignancies in Wilson disease. Liver Int. 2015;35:1615–22.
37. Roberts EA. Update on the diagnosis and management of Wilson disease. Curr Gastroenterol Rep. 2018;20:56.
38. Kim JW, Ye Q, Forgues M, Chen Y, Budhu A, Sime J, et al. Cancer-associated molecular signature in the tissue samples of patients with cirrhosis. Hepatology. 2004;39:518–27.
39. Sharma A, Seow JJW, Dutertre CA, Pai R, Blériot C, Mishra A, et al. Onco-fetal reprogramming of endothelial cells drives immunosuppressive macrophages in hepatocellular carcinoma. Cell. 2020;183:377–394.e21.
40. Veith A, Moorthy B. Role of cytochrome P450s in the generation and metabolism of reactive oxygen species. Curr Opin Toxicol. 2018;7:44–51.
41. Evans RM, Mangelsdorf DJ. Nuclear receptors, RXR, and the big bang. Cell. 2014;157:255–66.
42. Muchenditsi A, Yang H, Hamilton JP, Koganti L, Housseau F, Aronov L, et al. Targeted inactivation of copper transporter Atp7b in hepatocytes causes liver steatosis and obesity in mice. Am J Physiol Gastrointest Liver Physiol. 2017;313:G39–49.
43. Hao Y, Han L, Wu A, Bochkis IM. Pioneer factor Foxa2 mediates chromatin conformation changes for activation of bile acid targets of FXR. Cell Mol Gastroenterol Hepatol. 2024;17:237–49.
44. Chen J, Wang R, Xiong F, Sun H, Kemper B, Li W, et al. Hammerhead-type FXR agonists induce an enhancer RNA *Fincor* that ameliorates nonalcoholic steatohepatitis in mice. Elife. 2024;13:RP91438.
45. Mordaunt CE, Kieffer DA, Shibata NM, Członkowska A, Litwin T, Weiss KH, et al. Epigenomic signatures in liver and blood of Wilson disease patients include hypermethylation of liver-specific enhancers. Epigenetics Chromatin. 2019;12:10.
46. Pierson H, Muchenditsi A, Kim BE, Ralle M, Zachos N, Huster D, et al. The function of ATPase copper transporter ATP7B in intestine. Gastroenterology. 2018;154:168–180.e5.
47. Sarode GV, Mazi TA, Neier K, Shibata NM, Jospin G, Harder NHO, et al. The role of intestine in metabolic dysregulation in murine Wilson disease. Hepatol Commun. 2023;7:e0247.
48. Mazi TA, Sarode GV, Czlonkowska A, Litwin T, Kim K, Shibata NM, et al. Dysregulated choline, methionine, and aromatic amino acid metabolism in patients with Wilson disease: Exploratory metabolomic profiling and implications for hepatic and neurologic phenotypes. Int J Mol Sci. 2019;20:5937.
49. Sauerbruch T, Hennenberg M, Trebicka J, Beuers U. Bile acids, liver cirrhosis, and extrahepatic vascular dysfunction. Front Physiol. 2021;12:718783.
50. Ali RO, Haddad JA, Quinn GM, Zhang GY, Townsend E, Scheuing L, et al. Taurine-conjugated bile acids and their link to hepatic S1PR2 play a significant role in hepatitis C-related liver disease. Hepatol Commun. 2024;8:e0478.

How to cite this article: Wooton-Kee CR, Yalamanchili HK, Mohamed I, Hassan M, Setchell KD, Narvaez Rivas M, et al. Changes in the FXR-cistrome and alterations in bile acid physiology in Wilson disease. Hepatol Commun. 2025;9:e0707. https://doi.org/10.1097/HC9.0000000000000707